Electronic Supplementary Material (ESI) for ChemComm.

Electronic Supplementary Information for:

Zero-dimensional Cu(I)-based Organometallic Halide with Green Cluster-Centred Emission for High Resolution X-Ray Imaging Screens

Alaa M. Almushaikeh[a], Hong Wang[a], Luis Gutiérrez-Arzaluz[a], Jun Yin[b], Ren-Wu Huang[a], Osman M. Bakr[a], and Omar F. Mohammed[a]*

[a] Division of Physical Sciences and Engineering, King Abdullah University of Science and Technology (KAUST), Thuwal 23955-6900, Kingdom of Saudi Arabia

[b] Department of Applied Physics, The Hong Kong Polytechnic University, Kowloon 999077, Hong Kong, P. R. China

* Email: omar.abdelsaboor@kaust.edu.sa

Contents

Section S1. Experimental section

Reagents

Copper(I) iodide (CuI, 99%, Sigma-Aldrich), rubidium iodide (RbI, 99%, Macklin), 18-crown-6 ($C_{12}H_{24}O_6$, 99%, Sigma-Aldrich), poly(methyl methacrylate) (PMMA, Sigma-Aldrich), hypophosphorous acid (H_3PO_2, 50% in water by weight, Sigma-Aldrich), acetone (C_3H_6O, 99.5%, Sigma-Aldrich) and chloroform ($CHCl_3$, 99%, Sigma-Aldrich). All chemicals were used directly as received.

Synthesis

Synthesis of [Rb(18-crown-6)]$_2$Cu$_4$I$_6$·acetone (RCCI·acetone) single crystal. CuI (0.5 mmol), RbI (0.5 mmol), 18-crown-6 (0.5 mmol), and H_3PO_2 (1 mL) were dissolved in acetone (3 mL) at room temperature and stirred to form a clear-yellowish solution. Crystals were then obtained by storing the solution in a 254 K freezer for 12 h.

Synthesis of [Rb(18-crown-6)]$_2$Cu$_4$I$_6$ (RCCI) microcrystalline powder. The microcrystalline powder was synthesized by manually grinding 476 mg of Cu(I)I, 530 mg of RbI, and 660 mg of 18-crown-6 using a mortar and a pestle, a pale-yellow microcrystalline powder was then obtained.

Preparation of 50 wt.% RCCI@PMMA imaging screens. 200 mg of RCCI microcrystalline powder was dispersed in 2 mL of chloroform for 5 min, then 200 mg of PMMA was added and dispersed for 2 h. The viscous solution was then placed in a shaker for 3 h. The homogenous solution is then drop-casted in a glass petri dish that was used as a mold, the petri dish was then covered with aluminum foil and left overnight to evaporate the chloroform. After the solvent is evaporated, the imaging screen is slowly peeled off the petri dish by using a tweezer.

Methods

Single-crystal X-ray Diffraction (SCXRD) Single-crystal X-ray diffraction data were collected using a Bruker X8 PROSPECTOR APEX2 CCD diffractometer (Mo Kα, λ = 0.71073 Å) at 260 K. Data processing was performed using Bruker's APEX3 software. [1] Data integration and reduction were performed using SaintPlus. [2] Absorption corrections were performed by the multi-scan method implemented in SADABS-2016/2. [3] Space groups were determined using XPREP implemented in APEX3. [1] The structures were solved with the ShelXT[4] structure solution program using intrinsic phasing and refined with the ShelXL-2015[5] refinement package by least squares minimization using Olex2. [6] All non-hydrogen atoms were located in difference-Fourier maps and were then refined anisotropically. All hydrogen atoms were assigned isotropic displacement coefficients U(H) = 1.2U or 1.5U, and their coordinates were allowed to ride on their respective atoms.

Powder X-ray diffraction (PXRD) measurement was carried out with a Bruker D8 Advance diffractometer, using CuKα radiation in the 2θ range of 2–70° at a 2θ step of 0.02° and a counting time of 0.3-2 s per step.

Steady-state Photoluminescence (PL) spectra of the imaging screens were recorded by Horiba Fluoromax-4 spectrofluorometer with a photomultiplier (PMT-928).

PLQY measurement was carried out using an Edinburgh Instruments FLS920 Fluorescence Spectrometer equipped with 450 W continuous wavelength xenon lamp and an integrating sphere.

SEM and EDX analysis were conducted using a Zeiss Auriga high-resolution scanning electron microscope equipped with EDX detector to analyze the morphologies and chemical compositions of the powder.

The thermal degradation behavior of RCCI was characterized using thermogravimetric analysis (TGA, Discovery Series, TA Instruments).

The absorption spectrum was collected using a UV–vis–NIR spectrophotometer (PerkinElmer, Lambda 950, USA) at room temperature.

Time-Resolved Photoluminescence measurements were conducted using a Time-Correlated Single-Photon Counting (TCSPC) system. Measurements on the imaging screen samples were performed in a setup based on a modified microscope (Olympus IX71). The samples were placed over cleaned quartz coverslips and were excited at 405 nm with a pulsed diode laser (70 ps, HORIBA, Delta Diode) focused through a 10×, 0.4 NA microscope objective (Olympus) that was also used to collect the PL. The interpulse duration was set to be longer than the PL decay time (50 kHz) to ensure complete relaxation, and the intensity of the pulses was adjusted to be 16 nW with a set of neutral density filters (Thorlabs) to ensure that less than 1% of the excitation events resulted in the detection of a single photon. 490-nm long-pass filter (Newport) was used to reject scattered laser light and select the emission detection range. The filtered PL signal was focused on an avalanche photodiode (PDM series, MicroPhoton Devices). TCSPC data was collected using HydraHarp 400 electronics (PicoQuant). The overall system's time resolution was better than 150 ps. The histograms obtained were fitted with the SymphoTime64 software (PicoQuant), using the Levenberg– Marquardt iteration algorithm.

Radioluminescence (RL) Measurement. The RL spectra were taken by a spectrometer (Horiba Fluromax-4) equipped with an X-ray tube (Tungsten target, Moxtek). The detection slit was set at 5 nm, and the X-ray outlet was set to 1 cm away from sample for all spectral measurements. The X-ray dose rate was controlled in a range from 3.43 µGy/s to 31.63 mGy/s by adjusting the input current and voltage values. All tests were carried out in a radiation-tight environment of lead-plate shielding.

Temperature-dependent PL and RL measurements. Temperature dependent PL and RL measurements by Horiba Fluromax-4 spectrofluorometer assisted by Janis cryogenic chamber.

Femtosecond Transient Absorption (fs-TA) measurements. The fs-TA measurements of the samples were obtained in a Helios spectrometer (Ultrafast Systems). For this purpose, the imaging screen samples were excited with pump pulses at 400 nm, generated after passing through a fraction of an 800 nm beam (Astrella, Coherent, ~150 *fs* pulse,1 kHz, 7 mJ/pulse) into the spectrally tunable optical parametric amplifier (Newport Spectra-Physics). The probe pulses (UV visible and NIR wavelength continuum, white light) were generated by passing another fraction of the 800 nm pulses through a 2-mm CaF_2 crystal. Before the white light was generated, the 800 nm amplified pulses were passed through a motorized delay stage. Depending on the

movement of the delay stage, the transient species were detected following excitation at different time scales. The white light was split into two beams (signal and reference) and focused on two fiber optics to improve the signal-to-noise ratio. The excitation pump pulses were spatially overlapped with the probe pulses on the samples after passing through a synchronized mechanical chopper (500 Hz) which blocked alternative pump pulses. The absorption change (ΔA) was measured based on the time delay and wavelength (λ).

Calculation of X-ray Detection Limit. The linear relationship between the RL intensity of the corresponding samples and the X-ray dose was obtained. The noise data were obtained in the absence of sample. The noise intensity value was statistically analyzed and fitted by the Gaussian function, whereby the FWHM was regarded as the average value of the noise. The detection limit in dose rate was derived from the slope of the fitting line, with a signal-to-noise ratio of 3.

X-ray Image Collection and Processing. A commercial camera (D7100, Nikon) was used to take images for the flexible, large-area X-ray imaging screens. The ISO, aperture, and shutter were set at 200, F4, and 15 for samples excited by X-ray. The voltage/current of the X-ray tube was set to 50 kV/200 μA. The original X-ray images were further processed using the software Image J to remove the background of the screen.

Calculation of X-ray Imaging Spatial Resolution. X-ray Imaging spatial resolution was calculated by Modulation transfer function (MTF) measurements. The MTF was calculated by the slanted edge method. Sharp edge X-ray imaging was carried out on the standard line-pair lead template with a thickness of ~ 0.5 mm. MTF operation on images through software Image J: Then the edge spread function (ESF) was derived from the edge image, and the line spread function (LSF) was derived from the derivation. Finally, the Fourier transform of LSF defined MTF. The summary was shown in the following formula:

$$MTF(v) = F(LSF(x)) = F(\ dESF(x) \ / \ dx\ )$$

Where v was the spatial frequency and X is the position of pixels.

Computational methods.

The density functional theory (DFT) calculations were performed by using the generalized gradient approximation (GGA) approach and the Perdew-Burke-Ernzerhof (PBE) functional as implemented in Vienna ab initio simulation package (VASP).[7-8] The crystal structure of orthorhombic-phase RCCI was optimized with plane-wave basis set cutoff of 400 eV together with the uniform Brillouin zone grid of 1×2×2 k-mesh. The atomic positions were fully relaxed until the total Hellmann-Feynman forces in each atom were less than 0.02 eV/Å. The electronic band structures and projected density of states for RCCI were calculated with the same settings.

Section S2. Supplemental Figures and Tables.

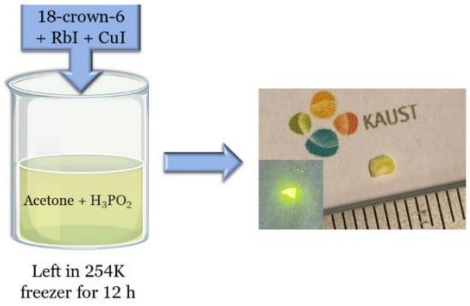

Fig. S1. Schematic illustration of the synthesis of RCCI·acetone crystal, RCCI·acetone crystal in ambient light and under UV-excitation.

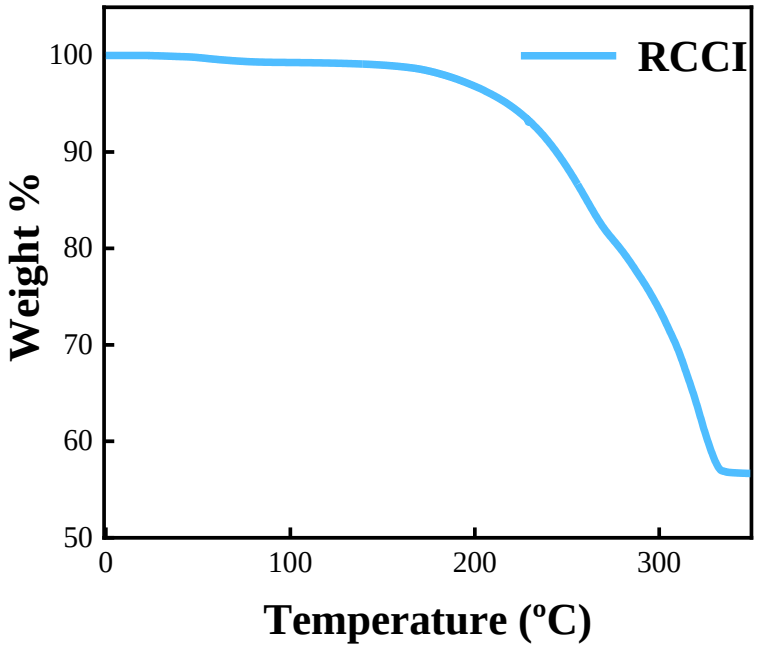

Fig. S2: Thermogravimetric analysis (TGA) curve of pure RCCI powder.

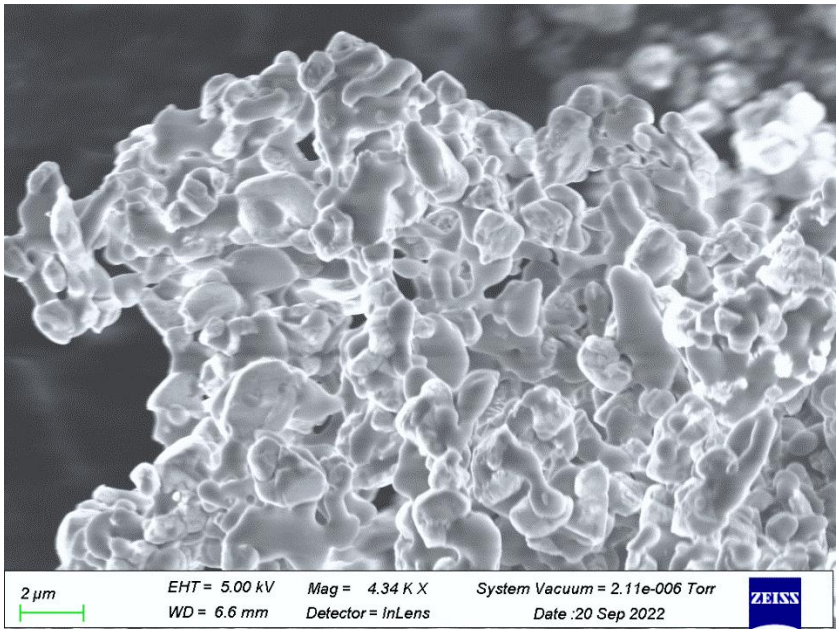

Fig. S3: SEM image of RCCI pure powder.

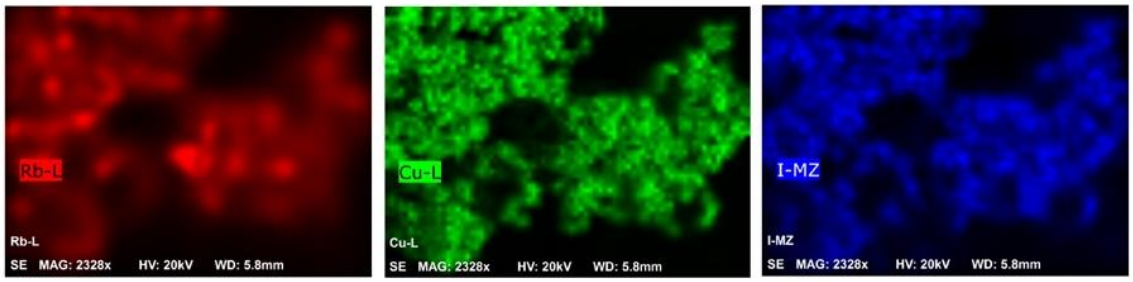

Fig. S4: Energy dispersive X-ray spectroscopy (EDX) elemental mapping of RCCI powder.

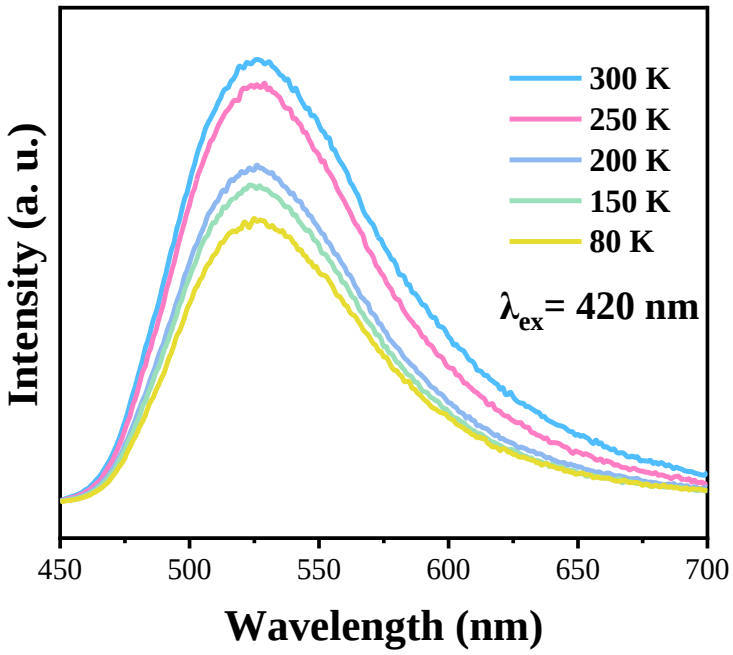

Fig. S5: Temperature-dependent PL spectra (80 K-300 K) of 50 wt.% RCCI@PMMA imaging screens.

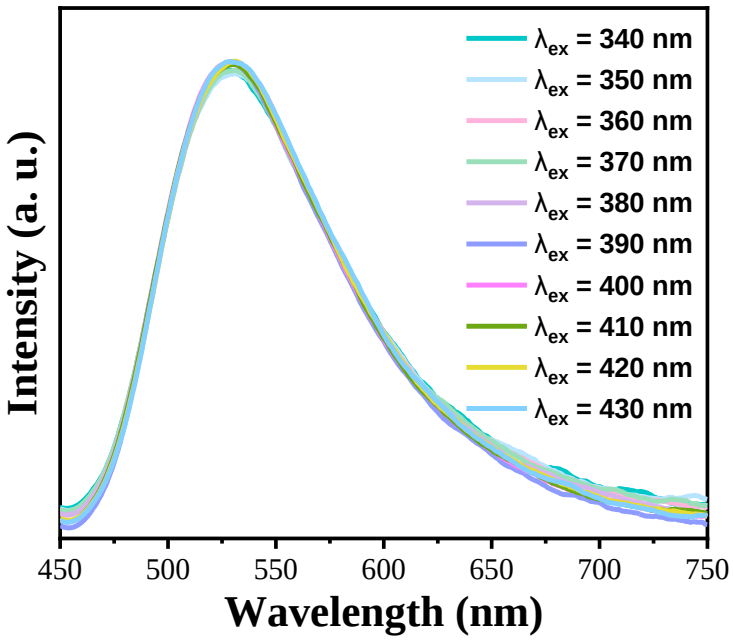

Fig. S6: Normalized photoluminescence spectra of 50 wt.% RCCI@PMMA imaging screens under various excitation wavelengths.

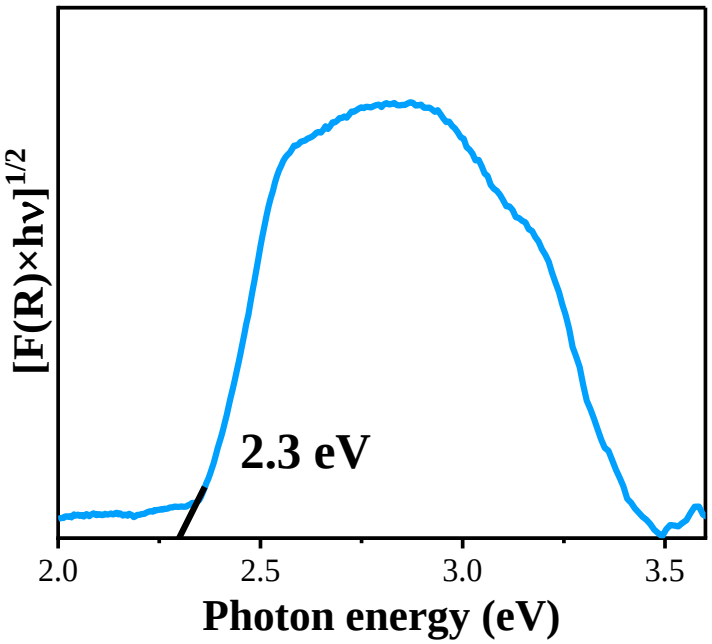

Fig. S7: The diffuse reflection spectrum of 50 wt.% RCCI@PMMA imaging screens.

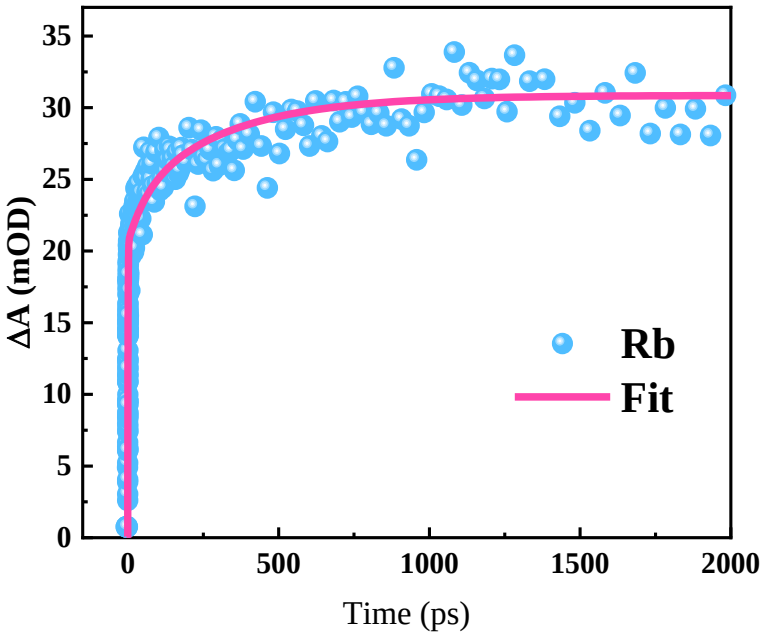

Fig. S8: *fs*-TA kinetic trace of 50 wt.% RCCI@PMMA imaging screens imaging screen excited at 400 nm. λ_{det} = 550 nm.

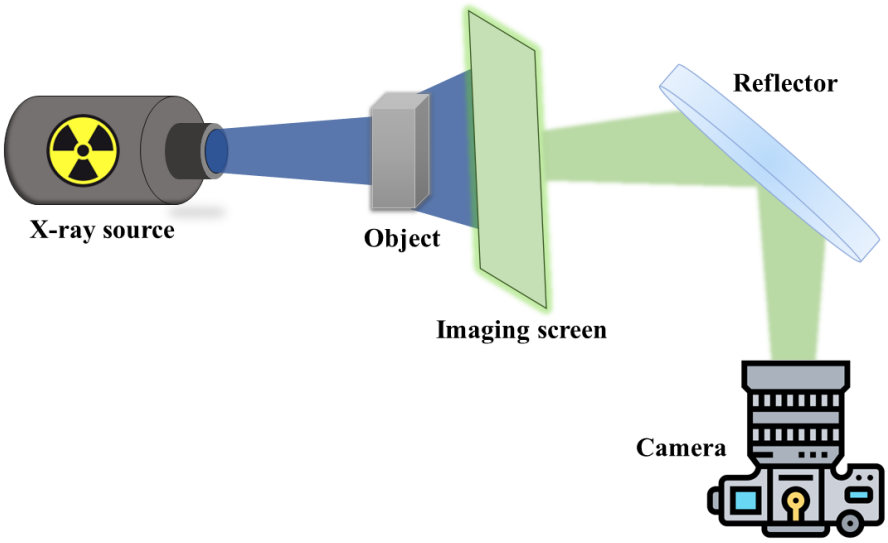

Fig. S9: An illustration scheme of the home-made X-ray imaging system.

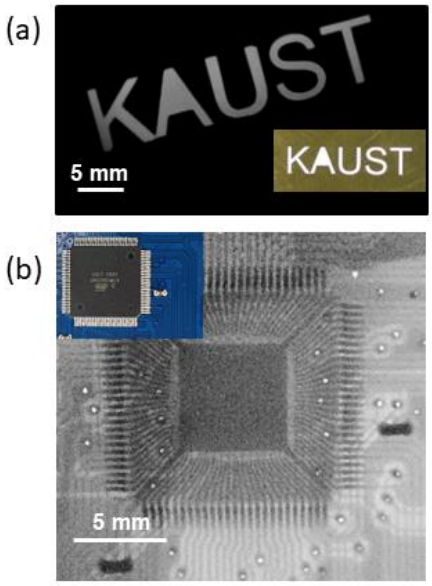

Fig. S10: X-ray images recorded under 50 kV using 50 wt.% RCCI@PMMA imaging screens imaging screens. (a) Engraved shadow mask of brass. (b) CPU card showing the internal components; inset is the ambient images.

Table S1. Main crystal structure parameters of RCCI·acetone Single Crystal.

Chemical formula	$C_{27}H_{54}Cu_4I_6O_{13}Rb_2$
Abbreviation	RCCI·acetone
Molecular weight	1773.20
Temperature (K)	260 K
Crystal system	Orthorhombic
Space group, Z	Pnma
a (Å)	30.8880(15)
b (Å)	15.2430 (8)
c (Å)	10.9290(6)
α (°)	90.0000°
β (°)	90.0000°
γ (°)	90.0000°
V (Å³)	5145.66(5)
ρ_{calc} ***(g/cm³)***	2.28884
μ (mm⁻¹)	7.157
Reflections collected	48331
Independent reflections	8048
R_{int}	*0.0372*
R_{sigma}	*0.0282*
F(000)	3312.0
Index ranges	$-42 \le h \le 44$, $-21 \le k \le 21$, $-15 \le l \le 14$
Data/restraints/parameters	8048/599/426
2θ range for data collection (°)	4.566 to 60.942
R1 [I>=2σ (I)]	R1 = 0.0401, wR2 = 0.0838
Final R indexes [all data]	R1 = 0.0732, wR2 = 0.1103
Largest diff. peak/hole (e Å^{-3})	0.87/-1.04
Goof	1.063
Radiation	MoKα (λ = 0.71073)
CCDC number	2237940

SI References

1. APEX3 (Bruker AXS Inc, Madison, Wisconsin, USA, **2018**).
2. SAINT (Bruker AXS. Inc, Madison, Wisconsin, USA, **2018**).
3. SADABS, empirical absorption correction program. Sheldrick, G.M. Bruker ASX Inc, Madison, Wisconsin, USA, **2002**.
4. Sheldrick, G. M. SHELXT – Integrated space-group and crystal structure determination. *Acta Cryst.* A. 71, 3–8 (**2015**)
5. Sheldrick, G. M. Crystal structure refinement with SHELXL. *Acta Cryst*. C. 71, 3–8 (**2015**)
6. Dolomanov, O. V., Bourhis, L. J., Gildea, R. J., Howard, J. A. K. & Puschmann, H. OLEX2: a complete structure solution, refinement, and analysis program. *J. Appl. Cryst.* 42, 339–341 (**2009**).
7. Kresse, G.; Furthmuller, J. Efficient Iterative Schemes for Ab Initio Total-Energy Calculations Using a Plane-Wave Basis Set. *Phys. Rev.* B **1996**, 54, 11169-11186.
8. Kresse, G.; Joubert, D. From Ultrasoft Pseudopotentials to the Projector Augmented-Wave Method. *Phys. Rev.* B **1999**, 59, 1758-1775.